

# Young massive star clusters in M51

Søren S. Larsen

*UC Observatories / Lick Observatory, University of California  
Santa Cruz, CA 95064, USA  
email: soeren@ucolick.org*

27 October 2018

## ABSTRACT

A search for young massive star clusters (YMCs) in the nearby face-on spiral galaxy M51 (NGC 5194) has been carried out using  $UBV$  CCD images from the prime focus camera on the Lick 3 meter Shane telescope. The YMC population is found to be quite rich with a specific  $U$ -band luminosity  $T_L(U) \sim 1.4$ , consistent with the high current star formation rate of this galaxy. The brightest clusters have  $M_V \sim -12.5$ , far brighter than any young clusters currently known in the Milky Way and even surpassing the luminosity of the R136 cluster in the 30 Dor complex in the Large Magellanic Cloud. A few of the YMCs are examined on archive HST/WFPC2 images, confirming their cluster nature and providing estimates of their effective radii of 2–3 pc. The number of YMCs in M51 is compatible with extrapolation of a power-law luminosity function with exponent  $\sim -2$  from a Milky Way-like population of open clusters. Both the SFR and  $T_L(U)$  of M51 are similar to those of other cluster-rich spiral galaxies like NGC 1313 and M83.

**Key words:** galaxies: spiral – galaxies: star clusters – galaxies: individual (NGC 5194) – galaxies: interactions

## 1 INTRODUCTION

M51 is probably among the most famous galaxies in the sky, instantly recognizable by its nearby companion NGC 5195. Also known as the “Whirlpool Galaxy”, it was one of the first galaxies in which spiral structure was discovered by Lord Rosse, and it provides a spectacular text-book example of a grand-design Sbc type spiral seen nearly face-on. It has a very high optical surface brightness (Okamura et al. 1976) and is also a strong emitter of far-infrared radiation, indicating strong star formation activity in the spiral arms (Smith 1982; Hippelein et al. 1996). Deep images reveal faint outlying material embedding both M51 and NGC 5195 (Burkhead 1978), providing clear evidence that the two galaxies are physically interacting. These characteristics, along with the relatively small distance ( $8.4 \pm 0.6$  Mpc, Feldmeier et al. 1997) and the location far from the galactic plane ( $b = 68^\circ$ ) make M51 an attractive target for studying its population of *Young Massive Star Clusters* (YMCs).

YMCs are abundant in interacting and merger galaxies like e.g. the “Antennae” NGC 4038/4039 (a list of galaxies with known YMC populations is given in Larsen (1999b)). However, they are also seen in more normal galaxies like e.g. the LMC (van den Bergh 1991) and M33 (Christian & Schommer 1988). In a recent study of 21 nearby, non-interacting spiral galaxies, Larsen & Richtler (2000) (LR2000) found a strong correlation between the specific

$U$ -band luminosity  $T_L(U)$  of YMCs in a galaxy and the area-normalized star formation rate  $\Sigma_{\text{SFR}}$ . In this respect, M51 provides a highly interesting intermediate case of a clearly interacting galaxy that has still retained the characteristics of a normal spiral.

This paper reports the results of a study of YMCs in M51. In Sect. 3, YMCs are identified and photometry is obtained from ground-based  $UBV$  CCD imaging. Archive HST/WFPC2 images are then used to examine a few clusters in detail, including measurements of their sizes (Sect. 4). Next, the specific  $U$ -band luminosity of the M51 cluster system is derived and compared with other galaxies (Sect. 5). In Sect. 6 the YMC population in M51 is compared with young clusters in the Milky Way and the LMC, along with some considerations on formation of YMCs. Finally, conclusions are in Sect. 7.

## 2 DATA

### 2.1 Observations and initial reductions

CCD images in the  $UBV$  passbands were obtained on Mar 13–14, 2000 with the prime focus camera (PFCAM) on the Lick 3 meter Shane telescope at Mount Hamilton, California. The total integration times were 3600, 1200 and 900 sec. in  $U$ ,  $B$  and  $V$ , split into 3 individual exposures in each filter. Typical seeing values ranged between  $1''.0$  and  $1''.5$ ,

arXiv:astro-ph/0008191v1 14 Aug 2000

**Table 1.** HST archive images of M51 used for photometric calibration of ground-based photometry.

| PID  | PI        | Filter | Exposure times |
|------|-----------|--------|----------------|
| 5777 | Kirschner | F555W  | 600 s          |
| 5777 | Kirschner | F439W  | 2 × 700 s      |
| 5652 | Kirschner | F336W  | 3 × 400 s      |

but the image quality was degraded by problems with the alignment of the mirror cell after recent re-aluminization and oscillations due to wind, making stellar images appear somewhat elongated. The image scale was  $0''.296$  /pixel and the total field of view was  $10' \times 10'$ , sufficient to fully cover both M51 itself and the companion NGC 5195.

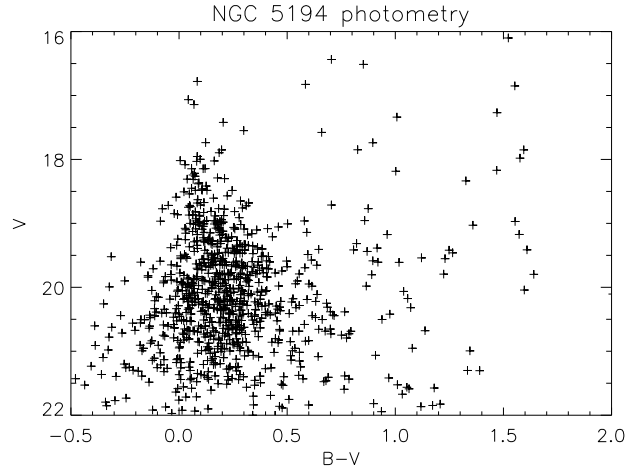
To reduce read-out time, the two halves of the CCD were read out in parallel through two amplifiers. During the subsequent reductions, the difference between the bias levels in the two parts of the CCD image was found to change by up to  $\sim 40$  ADU from one exposure to another. The difference was eliminated by adding a constant number to all pixel values in one half of the image. A more serious concern was that the flat-field varied significantly, most likely because of scattered light. Dividing two skyflats in the same filter with each other, the ratio was found to vary by up to  $\sim 20\%$  from the centre to the corner of the chip, with the most severe problems in the southern  $\sim 300$  pixels (about  $1.5'$ ) of the field. Within the central  $1000 \times 1000$  pixels the variations were less dramatic, but still quite significant at about the 5% level. The effect was clearly visible in the final calibrated images as large-scale gradients in the background. However, the pattern appeared to be more or less the same in all passbands so the flatfielding errors may, to a certain extent, cancel out for colour indices.

## 2.2 Photometric calibration

Standard fields from Landolt (1992) were observed for photometric calibration. The transformation equations were assumed to be of the form

$$\begin{aligned} V &= v + c_v \times (b - v) + z_v \\ B - V &= c_{(b-v)} \times (b - v) + z_{(b-v)} \\ U - B &= c_{(u-b)} \times (u - b) + z_{(u-b)} \end{aligned}$$

where capital letters denote standard magnitudes and small letters indicate instrumental magnitudes, corrected for atmospheric extinction. However, because of non-photometric conditions and the flat-field problems it was necessary to correct the zero-points of the  $UBV$  photometry using HST archive images.  $UBV$  magnitudes were obtained for sources in the HST images listed in Table 1, following the standard procedure described in Holtzman et al. (1995). Objects bright enough to be used for calibration of the ground-based images were easily measured through the Holtzman et al. reference aperture of  $r = 5$  pixels, avoiding problematic aperture corrections. The zero-points ( $z_v$ ,  $z_{(b-v)}$  and  $z_{(u-b)}$ ) of the ground-based magnitudes were then adjusted to fit the HST system, while the scaling constants ( $c_v$ ,  $c_{(b-v)}$  and  $c_{(u-b)}$ ) derived from the Landolt standard fields were preserved. The overlap between the HST datasets used for the  $BV$  and  $U$  calibrations amounted to less than the area of

**Figure 1.**  $(B-V, V)$  colour-magnitude diagram for objects in the M51 field. Objects with  $B-V > 0.5$  are mostly foreground stars whereas contamination blueward of  $B-V = 0.5$  is expected to be small.

one WF camera chip, making it difficult to find a suitable number of calibration objects. The  $U-B$  calibration is thus somewhat more uncertain than the  $B-V$  and  $V$ -band calibrations and it is estimated that  $z_{(u-b)}$  is good to  $\pm 0.15$  mag while  $z_{(b-v)}$  is probably accurate to better than  $\pm 0.05$  mag. Although significantly worse than what could have been obtained under optimal photometric conditions, the calibrations adopted here are nevertheless accurate enough for the conclusions drawn in this paper.

## 3 SELECTION OF CLUSTER CANDIDATES

In order to facilitate a comparison with the results of LR2000, the same data reduction and analysis procedures were followed as closely as possible. Objects were detected using the DAOFIND task in DAOPHOT (Stetson 1987) on background-subtracted  $V$  and  $B$  band images and matching the two object lists. Aperture photometry was then carried out as described in Larsen (1999a), using an aperture radius of  $r = 5$  pixels. Finally, a correction for interstellar absorption of  $A_B = 0.150$  mag was applied (Schlegel et al. 1998).

The resulting  $(B-V, V)$  colour-magnitude diagram is shown in Fig. 1. An initial list of cluster candidates was then obtained by selecting all objects with

- $B - V < 0.45$
- $M_V < \begin{cases} -9.5 & \text{for } U - B < -0.4 \\ -8.5 & \text{for } U - B \geq -0.4 \end{cases}$

These criteria ensure minimal contamination from foreground stars, the majority of which will be redder than the  $B-V$  cut, and by individual luminous stars in M51 itself because of the  $M_V$  limit. However, many of the objects identified in this way were still not likely cluster candidates, but high-surface brightness parts of spiral arms, HII regions or just artefacts found by DAOFIND where no real object existed. A visual inspection of the images, looking for relatively isolated, point-like sources, was found to be the only

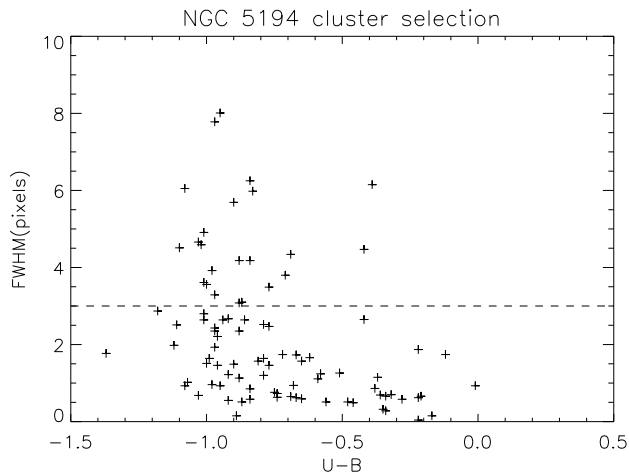


**Figure 2.** The intrinsic FWHM vs.  $U-B$  colour for cluster candidates in M51 that passed the initial visual inspection. The horizontal dashed line indicates the size cut applied to further constrain the cluster sample.

way to isolate good cluster candidates from the multitude of other objects in the frames.

LR2000 further used  $H\alpha$  images to reject the youngest objects, still embedded in HII regions and often surrounded by a fuzz of nebular emission and star forming regions, but no  $H\alpha$  filter was available at PFCAM during this observing run. Instead, such objects were rejected based on their angular sizes. Object sizes were measured using the ISHAPE algorithm (Larsen 1999a), convolving the point spread function (PSF) of the  $V$ -band image with King profiles to match the observed object profiles. A concentration parameter of 30 was assumed for the King profiles. Fig. 2 shows the intrinsic object sizes derived by ISHAPE as a function of  $U-B$  colour for objects that passed the initial visual inspection. Clearly, most of the more extended sources are found among the bluest objects, while most objects with  $U-B \gtrsim -0.6$  have  $\text{FWHM} < 2$  pixels. Note that the typical seeing in our images corresponds to  $\text{FWHM} \sim 5$  pixels. A size cut at  $\text{FWHM}=3$  pixels was finally applied to exclude the fuzziest objects, likely to be OB associations or HII regions rather than real star clusters.

Although the cluster colours have been corrected for Galactic foreground extinction, some residual reddening may still be present from M51 itself. The question of the optical thickness of face-on spiral galaxies is still debated, and for any particular object the absorption will obviously depend on the local structure of the surrounding interstellar medium. However, a recent study (Xilouris et al. 1999) concluded that face-on spiral galaxies are essentially transparent with an optical depth of less than one in all optical bands. M51 being obviously face-on (inclination angle  $\sim 20^\circ$ , Tully 1974), interstellar extinction problems are thus expected to be small.

The final list consists of 69 cluster candidates (Table 3). A  $(B-V, U-B)$  diagram for these is shown in Fig. 3, along with stellar models by Bertelli et al. (1994) and the Girardi et al. (1995) “S”-sequence which marks the average colours of LMC clusters. The arrow indicates the effect of a reddening of 0.3 in  $B-V$ , equivalent to 0.93 magnitudes of  $V$ -band absorption for a standard reddening law. The M51

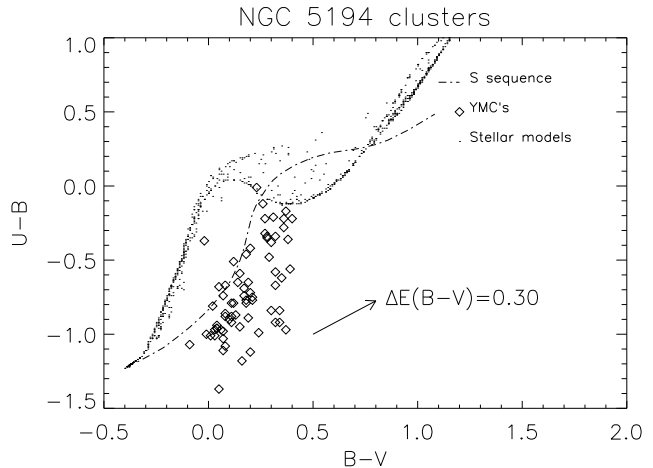


**Figure 3.**  $(B-V, U-B)$  two-colour diagram for the final sample of cluster candidates in M51

clusters tend to have somewhat bluer  $U-B$  colours than expected from the S-sequence, but a shift of about 0.1 in  $U-B$  would make them match the S-sequence colours nicely. Such a shift would be consistent with the estimated uncertainties. The S-sequence is essentially an age sequence and Girardi et al. (1995) published a calibration of age as a function of position in the  $(B-V, U-B)$  diagram. However, because of the uncertainties in the photometric calibration and especially in the  $U$  band, a detailed discussion of ages for the M51 clusters will not be given in this paper, but note that the clusters do scatter along the S-sequence, indicating a significant age spread. Because of the fading with age, the sample becomes increasingly incomplete for higher ages. The upper age limit, due to the  $B-V$  cut, is about 500 Myr.

Fig. 4 shows a  $V$ -band image with the cluster positions indicated. Most of the cluster candidates are located in or near the spiral arms of M51 itself. This is to a large extent a selection effect, due to the fact that the youngest clusters are more luminous (for any given mass) and therefore easier to detect. However, note that also the companion galaxy contains a couple of massive clusters. The HST F439W + F555W pointing is also shown in Fig. 4.

## 4 HST DATA

In addition to being useful for calibrating the photometry, the superior angular resolution of the HST data provides a welcome way of examining the structure of the cluster candidates in much greater detail than what is possible from the ground. Fig. 5 shows WFPC/2 close-ups of 10 clusters, marked by asterisks (\*) in Table 3. The images in Fig. 5 are from two combined F439W exposures, allowing for cosmic ray rejection.

First, the HST images clearly confirm the cluster nature of most of the objects. Exceptions may be objects #627 – a quite faint source located near the nucleus of M51, and #597 and #403 which may consist of two or more closely separated individual stars. The remaining seven objects are far too bright to be individual stars and appear well resolved.

Most of the clusters are evidently not isolated objects, but are surrounded by individual luminous stars and other

**Table 2.** Comparison of ground-based and HST-based data for 7 clusters in M51. Cols. 2 and 3 list ground-based  $V$  and  $B-V$  magnitudes, Cols. 4 and 5 give the corresponding values measured on HST WFPC/2 images and the differences  $\Delta V = V(\text{ground}) - V(\text{HST})$  and  $\Delta B-V = B-V(\text{ground}) - B-V(\text{HST})$  are in Cols. 6 and 7. The colours given here have not been corrected for reddening. Effective cluster radii measured on the HST images are given in the last column.

| ID  | $V$ (ground) | $B-V$ (ground) | $V$ (HST) | $B-V$ (HST) | $\Delta V$ | $\Delta B-V$ | $R_e$ (pc) |
|-----|--------------|----------------|-----------|-------------|------------|--------------|------------|
| 403 | 19.58        | 0.342          | 19.80     | 0.29        | -0.22      | 0.05         | 2.7        |
| 477 | 18.41        | 0.210          | 18.46     | 0.33        | -0.05      | -0.12        | 0.9        |
| 479 | 18.11        | 0.098          | 18.83     | 0.06        | -0.72      | 0.04         | 3.8        |
| 534 | 19.48        | 0.177          | 20.24     | -0.04       | -0.76      | 0.22         | 2.3        |
| 589 | 19.40        | 0.070          | 19.51     | 0.08        | -0.11      | -0.01        | 2.1        |
| 597 | 19.90        | 0.177          | 19.72     | 0.52        | 0.18       | -0.34        | -          |
| 627 | 20.13        | 0.237          | 20.53     | 0.51        | -0.40      | -0.27        | 0.0        |
| 693 | 19.42        | 0.148          | 19.66     | 0.11        | -0.24      | 0.04         | 2.7        |
| 713 | 18.33        | 0.071          | 19.22     | -0.11       | -0.89      | 0.18         | 0.8        |
| 912 | 19.78        | 0.317          | 20.34     | 0.16        | -0.56      | 0.16         | 2.2        |



**Figure 4.** A  $V$ -band image of M51 with the cluster positions indicated. South is up. The large-scale variations in the background are due to poor flatfielding, presumably because of scattered light in the skyflats. The F439W / F555W HST pointing (PID 5777) is also shown.

clusters. This is, however, to be expected because most of these clusters have very blue  $U-B$  colours, indicating low ages. A  $U-B$  colour of  $-0.8$ , typical for the clusters in Fig. 5, corresponds to an age of about 12 Myr (Girardi et al. 1995), too short for a young star cluster to escape from the environment where it was born. The two reddest clusters (#693 and #912) with  $U-B = -0.59$  and  $U-B = -0.58$  already appear somewhat more isolated than the other clusters in the Fig. 5, consistent with the higher ages inferred from their  $U-B$  colours ( $\sim 30$  Myr).

#### 4.1 HST versus ground-based photometry

Table 2 lists HST-based photometry and sizes (see Sect. 4.2) for the 10 objects in Fig. 5. For comparison, ground-based

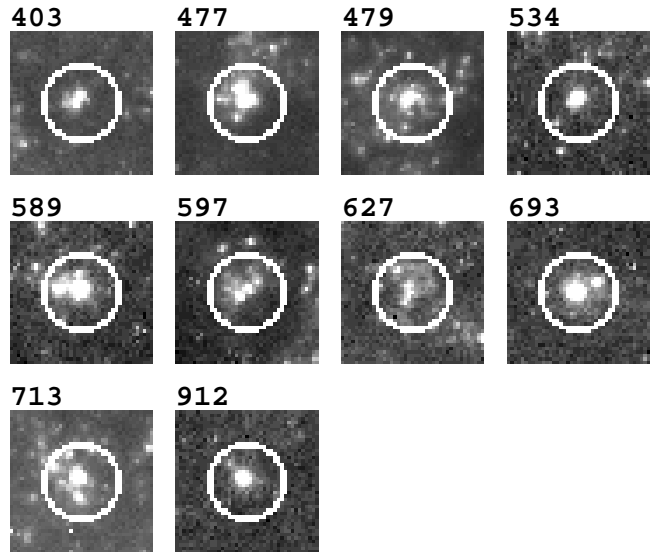


**Figure 5.** Clusters identified on HST images. The circles are 2 arcseconds in diameter.

photometry is also listed. The photometry in Table 2 has not been reddening corrected.

Magnitudes measured on the ground-based images are generally brighter than those based on HST images. This is not surprising, considering that the HST magnitudes were measured through a  $0''.5$  aperture which clearly does not include all the light surrounding the clusters that will enter into a ground-based aperture. Generally, the agreement on  $B-V$  colours is better than on  $V$  magnitudes, confirming that colours can be more accurately measured than individual magnitudes for objects in crowded fields. The difference between ground-based and HST-based  $B-V$  colours clearly increases for the fainter objects, with the largest discrepancy for the likely “non-clusters” (#597 and #627) pointed out above.

It is also worth noting that the HST pointings were centred on the nucleus of M51, providing a “worst-case” comparison between HST and ground-based data. Further out in the disk of M51 the surface brightness drops and the cluster sample becomes less biased towards the brightest (and thus youngest) objects where crowding problems are most significant.

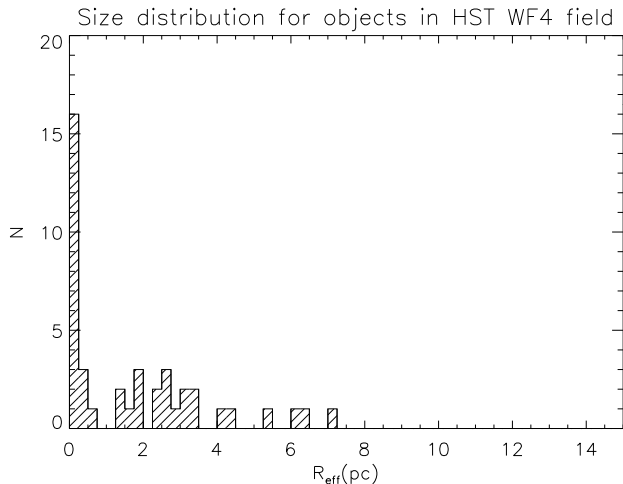


**Figure 6.** Histogram of the size distribution for objects in the WF4 chip of the combined F439W image.

#### 4.2 Cluster sizes

Sizes were measured on the WFPC/2 F439W images for the clusters in Fig. 5 with the ISHAPE algorithm (Larsen 1999a). At the distance of M51, one WF pixel corresponds to a linear scale of 4 pc, so measuring cluster sizes of the order of a few pc is not trivial. The input PSF for ISHAPE was generated empirically from point sources in the HST images, using the PSF task in DAOPHOT. This was preferred over generating the PSFs with the TINYTIM PSF simulator (Krist & Hook 1997) which does not include the so-called “diffusion kernel” for subsampled PSFs, and would thus have caused ISHAPE to derive too large cluster sizes.

The clusters were modelled as King profiles with concentration parameter  $c = 30$ , resulting in the half-light radii ( $R_e$ ) listed in the last column of Table 2. The cluster sizes measured here are consistent with sizes for YMCs in merger galaxies like the Antennae (Whitmore et al. 1999), with  $R_e \sim 2 - 3$  pc and do also match the typical size of *globular clusters* in the Milky Way and other galaxies quite well (Harris 1996). It has been estimated from simulations that ISHAPE is able to measure sizes down to  $\frac{1}{10}$  times the size of the PSF when sufficient signal is present (Larsen 1999a), corresponding to  $\sim 0.5$  pc in the current case. To illustrate the reliability of the cluster sizes, Fig. 6 shows a histogram of the size distribution for all objects brighter than  $V = 22$  in the WF4 chip. The histogram shows a narrow peak at  $R_e = 0$ , corresponding to unresolved point sources, while objects with sizes characteristic of the YMCs appear well separated from the  $R_e = 0$  peak. The YMCs are thus well resolved and their sizes are well determined.

## 5 GLOBAL PROPERTIES OF THE M51 CLUSTER SYSTEM

### 5.1 Specific luminosity

In studies of old globular cluster systems (GCSs) it has become customary to characterize the richness of a GCS by its *specific frequency*, originally defined by Harris & van den Bergh (1981) as the number of globular clusters ( $N_{GC}$ ) per

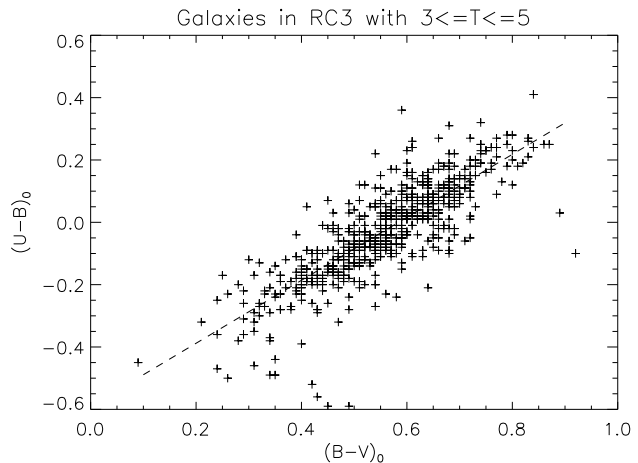


**Figure 7.**  $U-B$  vs.  $B-V$  for galaxies with  $T$ -type in the range 3 to 5 (from RC3). The dashed line is a fit to the data points.

host galaxy luminosity ( $M_V$ ):  $S_N = N_{GC} \times 10^{0.4 \times (M_V + 15)}$ . However, a potentially better measure is the specific *luminosity* (Harris 1991), which is the ratio of the total luminosity of the cluster system to that of the host galaxy. Specific luminosities are much less sensitive to incompleteness effects at the lower end of the cluster luminosity function because the fainter clusters obviously contribute less by light than they do by number. For YMC systems this advantage becomes even greater than for old GCSs because the faint wing of the cluster luminosity function is usually unknown, so a definition of an equivalent specific frequency for YMCs has to rely on artificial and somewhat arbitrary magnitude limits.

LR2000 defined the specific  $U$ -band luminosity for YMCs as follows:

$$T_L(U) = 100 \cdot \frac{L_{\text{Clusters}}(U)}{L_{\text{Galaxy}}(U)}, \quad (1)$$

where  $L_{\text{Clusters}}(U)$  and  $L_{\text{Galaxy}}(U)$  are the total  $U$ -band luminosities of the cluster system and of the host galaxy, respectively. The  $U$  band was chosen to sample the *young* cluster and stellar populations in a galaxy as cleanly as possible.

To calculate  $T_L(U)$  for M51,  $L_{\text{Clusters}}(U)$  was obtained simply by adding up the  $U$ -band light from all clusters in Table 3. Unfortunately, no integrated  $U$ -band photometry is available for M51 itself so its  $U$ -band magnitude was *estimated* from the  $BV$  photometry given in the RC3 catalogue (de Vaucouleurs et al. 1991). Fig. 7 is a plot of reddening-corrected  $(U-B)_0$  vs.  $(B-V)_0$  for all galaxies in RC3 with  $T$  types between 3 and 5, M51 itself being classified as Sbc ( $T = 4$ ). The data in Fig. 7 can be fitted by a straight line, yielding

$$(U-B)_0 = 1.01 \times (B-V)_0 - 0.59 \quad (2)$$

with a scatter of  $\sigma(U-B) = 0.09$  around the fit. The integrated  $(B-V)_0$  colour for M51 is given as 0.53 in RC3, so from Eq. (2) we get  $(U-B)_0 = -0.05$ . This should be accurate to 0.1 magnitudes, translating into a 10% uncertainty on the derived  $T_L(U)$  value. These  $(B-V)_0$  and  $(U-B)_0$  colours also compare well with integrated photometry for NGC 5236 (M83), a galaxy which is in many respects quite similar to M51. For NGC 5236, RC3 gives integrated

$(B-V)_0$  and  $(U-B)_0$  colours of 0.61 and  $-0.01$ , respectively, i.e. M51 is slightly bluer in both  $B-V$  and  $U-B$ .

The specific  $U$ -band luminosity of the M51 YMCs can now be obtained:

$$T_L(U) = 1.36 \pm 0.28 \quad (3)$$

Similarly, the  $V$ -band specific luminosity is found to be  $T_L(V) = 0.41 \pm 0.07$ . The errors quoted here are the formal errors due to sample statistics. The real uncertainties are probably higher, but are hard to estimate. For example, lowering the size cut to FWHM=2 pixels instead of 3 pixels would change  $T_L(U)$  to  $0.95 \pm 0.24$ . On the other hand, the M51 photometry does not go quite as deep as most of the galaxies in the sample of LR2000, – primarily because M51 is further away. Thus  $T_L(U)$  and  $T_L(V)$  are probably both somewhat underestimated.  $T_L(V)$  may be more affected because older, redder clusters carry more weight than for  $T_L(U)$ , while at the same time being fainter and therefore more incomplete.

## 5.2 The $T_L(U)$ vs. $\Sigma_{\text{SFR}}$ correlation

LR2000 found a very good correlation between  $T_L(U)$  and the area-normalized star formation rate  $\Sigma_{\text{SFR}}$  for the 21 galaxies in their sample and an additional 10 galaxies (mostly starbursts and merger galaxies) for which data were collected from the literature. How does M51 fit into this relation?

To derive  $\Sigma_{\text{SFR}}$  for M51, we use the relation from LR2000:

$$\Sigma_{\text{SFR}}(\text{M}_{\odot} \text{ yr}^{-1} \text{ kpc}^{-2}) = 144000 \times 10^{-0.4 m_{\text{FIR}} - 2 \log D_0}, \quad (4)$$

based on the calibration in Buat & Xu (1996).  $m_{\text{FIR}}$  is the RC3 FIR magnitude (based on IRAS  $60\mu$  and  $100\mu$  flux densities) and  $\log D_0$  is the logarithm of the optical galaxy diameter in tenths of arcminutes. Note that both  $\Sigma_{\text{SFR}}$  and  $T_L(U)$  are distance independent. In some cases the RC3 “effective aperture” ( $\log A_e$ ), containing half the  $B$ -band light, may provide a more reasonable measure of the area to which the SFR should be normalized, but this is not catalogued for all galaxies in RC3 and thus  $\log D_0$  was chosen for homogeneity.

For M51,  $m_{\text{FIR}} = 7.86$  and  $\log D_0 = 2.05$ . Inserting these numbers in (4), the star formation rate surface density is then

$$\Sigma_{\text{SFR}} = 8.21 \times 10^{-3} \text{M}_{\odot} \text{ yr}^{-1} \text{ kpc}^{-2} \quad (5)$$

This number is roughly a factor of two lower than the value given in Kennicutt (1998b), derived from the  $H\alpha$  luminosity. Considering the intrinsic uncertainties in both methods, the agreement is quite satisfactory.

The  $T_L(U) - \Sigma_{\text{SFR}}$  plot in LR2000 can now be updated with one more data point for M51, as shown in Fig. 8. M51 (labelled by its NGC number, 5194) fits quite nicely into the existing relation, with a  $T_L(U)$  comparable to other high  $\Sigma_{\text{SFR}}$  galaxies like NGC 1156 and NGC 1313. It may fall somewhat below the  $T_L(U)$  value expected for its  $\Sigma_{\text{SFR}}$ , but the error bars in the horizontal direction of Fig. 8 are probably substantial, with an uncertainty of at least 50% on the calibration of star formation rate as a function of FIR luminosity alone (Buat & Xu 1996).

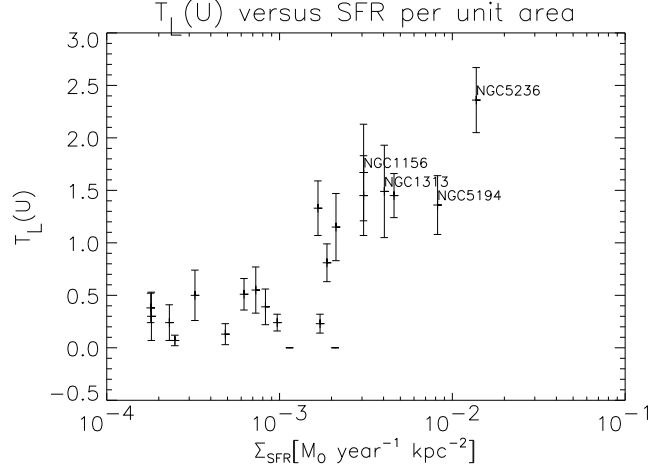


**Figure 8.** Specific  $U$ -band luminosity as a function of star formation rate surface density for galaxies in the sample of Larsen & Richtler (2000) and M51 (NGC 5194).

## 6 DISCUSSION

### 6.1 Comparison of the luminosity functions of YMCs in M51 and open clusters in the Milky Way

M51 contains a large number of very luminous star clusters, including 40 clusters with  $M_V < -10$  and 4 clusters with  $M_V < -12$  (Table 3). As indicated by Table 2, the ground-based  $V$  magnitudes are systematically brighter than the HST photometry, with an average difference of  $\Delta V = -0.38$  for the objects listed in Table 2. Applying a correction of 0.38 mag to all  $V$  magnitudes, M51 still contains 30 clusters with  $M_V < -10$  and 3 with  $V < -12$ . For comparison, the brightest known young clusters in the Milky Way have  $M_V \sim -10$  ( $h$  and  $\chi$  Persei, Schmidt-Kaler 1967; NGC 3603, van den Bergh 1978). Although it cannot be excluded, of course, that a few highly luminous clusters might be hiding in remote parts of the Galactic disk, it appears unlikely that the Milky Way contains any significant number of highly luminous clusters similar to those in M51. The brightest clusters in M51 even outshine the R136 cluster at the centre of the 30 Dor region in the LMC which has  $M_V = -10.6$  (van den Bergh 1978).

Do YMCs represent a separate class of objects, distinct from low-mass open clusters, or can YMC populations be reconciled with normal populations of low-mass clusters, assuming a standard power-law luminosity function (LF)? Let us compare the YMC population in M51 with the system of open clusters in the Milky Way, for the moment ignoring other differences between the two galaxies. van den Bergh & Lafontaine (1984) studied the luminosity function of Milky Way open clusters and found it to be well represented by the relation

$$\log \sigma(M_V) = 1.55 + 0.2M_V \quad (6)$$

for clusters fainter than  $M_V = -9$ , where  $\sigma(M_V)$  is the number of clusters per  $\text{kpc}^2$  per magnitude bin. In luminosity units, this becomes

$$n(L) \propto L^\alpha \quad (7)$$

where  $L$  is the luminosity,  $n(L)$  is the number of clusters per

luminosity bin and  $\alpha = -1.5$  (Elmegreen & Efremov 1997). In the Milky Way, extrapolation of (6) to higher luminosities would yield a total of  $\sim 100$  clusters with  $M_V = -11$ , assuming that the Galactic disk has an area of  $500 \text{ kpc}^2$ . This is clearly incompatible with what is actually observed and van den Bergh & Lafontaine (1984) suggested that the luminosity function of open clusters in the Milky Way drops below relation (6) somewhere in the magnitude range  $-11 < M_V < -8$ . In fact, there *must* be a drop-off in a luminosity function of the form (6) at some magnitude level, as the total luminosity of a cluster system with a power-law LF diverges for  $\alpha > -2$ . However, it is less obvious that the drop-off will occur at the same magnitude in all galaxies.

Young LMC clusters seem to follow a similar power-law LF with  $\alpha = -1.5 \pm 0.2$ , but the LF of young clusters declines more slowly at bright magnitudes than in the Milky Way (Elson & Fall 1985) due to the LMC's population of YMCs. So at least in the LMC, YMCs appear to mark a natural extension of the open cluster population to brighter magnitudes.

M51 contains 23 and 13 clusters in the two magnitude intervals  $-11 < M_V < -10$  and  $-12 < M_V < -11$ , respectively. If the  $\Delta V = 0.38$  correction is applied, the numbers are 20 clusters with  $-11 < M_V < -10$  and 6 clusters with  $-12 < M_V < -11$ . Most of the visible part of the disk of M51 is confined within a diameter of about  $6'$ , corresponding to an area of  $170 \text{ kpc}^2$ . Applying Eq. (6) to the two magnitude intervals above, 60 and 38 clusters would be expected – three times more than what is actually observed. Of course, the extrapolation of Eq. (6) to such bright magnitudes is very sensitive to the exact value of the exponent  $\alpha$ . Changing  $\alpha$  to  $-2$  instead of  $-1.5$  and using the Milky Way clusters in the magnitude bin  $-5 < M_V < -8$  for reference (5.2 clusters  $\text{kpc}^{-2}$ , van den Bergh and Lafontaine 1984), the predicted numbers drop to 6 clusters with  $-11 < M_V < -10$  and 2 in the interval  $-12 < M_V < -11$ , now several times below the observed numbers.

Although very crude, these calculations show that even though M51 is apparently much richer in *luminous* clusters than the Milky Way, the number of low-luminosity clusters in the two galaxies could still be quite similar without requiring any particularly peculiar luminosity function. The YMCs in M51 could easily be accommodated by simple extrapolation of a power-law luminosity function with an exponent somewhere between  $-1.5$  and  $-2$ , and there is apparently no need to conceive them as a separate class of objects.

## 6.2 Formation of massive clusters

From Fig. 8, M51 is indeed quite rich in YMCs compared to the “average” spiral galaxy. However, other spiral galaxies with similar rich YMC populations are known, and there is no particular evidence that the presence of YMCs in M51 is boosted by the interaction with NGC 5195. If anything, M51 may be slightly cluster-poor for its  $\Sigma_{\text{SFR}}$ . None of the other cluster-rich galaxies in the LR2000 sample show obvious signs of interaction, and the differences in their SFRs and  $T_L(U)$  values may be explained simply by different amounts of gas available for star formation (Kennicutt 1998a, LR2000). M51 itself is also very gas-rich (see e.g. table 1 in Kennicutt 1998b), consistent with its relatively high  $\Sigma_{\text{SFR}}$  and  $T_L(U)$  values.

Even higher levels of star forming activity are seen in merger galaxies like the Antennae (Whitmore et al. 1999) and NGC 3256 (Zepf et al. 1999), but also in starbursts that are not directly related to merger events like e.g. M82 (O’Connell et al. 1995) and NGC 5253 (Gorjian 1996). Such galaxies contain large numbers of highly luminous young clusters, emitting up to 15% of the blue or UV light (Meurer et al. 1995; Zepf et al. 1999) and mark an extension of the  $\Sigma_{\text{SFR}}-T_L(U)$  relation (LR2000). At the other extreme of the relation are galaxies like IC 1613 with exceedingly low (but non-vanishing) star formation rates and very few star clusters at all (Wyder, Hodge & Cole 2000).

It thus appears that galaxies form YMCs *whenever the SFR is high enough*. This may have important implications for the understanding of how massive clusters (aka *globular clusters*) formed in the early Universe. At earlier epochs, the general level of star forming activity was presumably higher because of the larger amounts of gas available, and globular clusters may have formed quite naturally. The highest levels of star forming activity may have existed at the centres of rich galaxy clusters, giving rise to the rich populations of globular clusters seen around many cD galaxies.

The key to understanding massive cluster formation may lie in the properties of the interstellar medium in their parent galaxies. In the Milky Way, star clusters form in the cores of highly fragmented giant molecular clouds (GMCs) (Lada et al. 1997), but at a very low efficiency averaged over the entire GMC. The largest GMCs in the Milky Way have masses of about  $5 \times 10^6 M_\odot$  with a sharp cut-off above this limit (McKee 1999). It is tempting to speculate that this upper cut-off may be related to the upper limit of the open cluster luminosity function discussed in the previous section. If massive clusters form with similar low efficiencies, their parent clouds must be much larger than Milky Way GMCs and it has been suggested that globular clusters formed from *supergiant molecular clouds* (SGMCs) with masses of  $10^8 - 10^9 M_\odot$  (Harris & Pudritz 1994). In M51 and NGC 5236, high-resolution CO studies have in fact revealed “Giant Molecular Associations” (GMAs) with masses of  $10^7 - 10^8 M_\odot$  (Vogel et al. 1988; Rand & Kulkarni 1990; Rand et al. 1999), which might be identifiable as the birth-sites of YMCs. Recently, Wilson et al. (2000) reported even more massive GMAs with masses of  $3 - 6 \times 10^8 M_\odot$  in the YMC-rich “Antennae” galaxies. Such GMAs may assemble more easily in galaxies with high gas densities and, consequently, high star formation rates (Kennicutt 1998a). The connection between SFR and YMC richness could then be understood as resulting from an underlying dependence of both on the gas density.

## 7 CONCLUSIONS

Young Massive Star Clusters (YMCs) have been identified in the nearby face-on Sbc-type spiral M51. The richness of the YMC population in M51, as measured by the specific  $U$ -band luminosity  $T_L(U)$  is comparable to other cluster-rich spiral galaxies, compatible with the high star formation rate in M51 and the  $\Sigma_{\text{SFR}} - T_L(U)$  relation (Larsen & Richtler 2000). The high level of star formation activity may in this particular case be partly stimulated by interaction with the nearby companion NGC 5195, but interactions do not in

general seem to be a necessary requirement for YMC formation.

Within order-of magnitude estimates, the number of YMCs in M51 is compatible with extrapolation of a power-law luminosity function with exponent  $\alpha \sim -2$  from a population of low-mass open clusters similar to that in the Milky Way. Thus, YMCs may simply represent a continuation of the normal open cluster luminosity function, extending to different upper limits in different galaxies. Therefore YMCs plausibly form in much the same way as lower-mass clusters and it appears likely that these same basic mechanisms also applied to the formation of globular clusters in the early Universe.

## 8 ACKNOWLEDGMENTS

This work was supported by National Science Foundation grant number AST9900732 and Faculty Research funds from the University of California, Santa Cruz.

## REFERENCES

- Bertelli G., Bressan A., Chiosi C., Fagotto F., Nasi E., 1994, *A&AS*, 1006, 275
- Buat V., Xu C., 1996, *A&A*, 306, 61
- Burkhead M. S., 1978, *ApJS*, 38, 147
- Christian C. A., Schommer R. A., 1988, *AJ*, 95, 704
- de Vaucouleurs G., de Vaucouleurs A., Corwin H. G. Jr., Buta R. J., Paturel G., Fouque P., 1991, "Third Reference Catalogue of Bright Galaxies", Springer-Verlag New York
- Elmegreen B. G., Efremov Yu. N., 1997, *ApJ*, 480, 235
- Elson R. A. W., Fall S. M., 1985, *PASP*, 97, 692
- Feldmeier J. J., Ciardullo R., Jacoby G. H., 1997, *ApJ*, 479, 231
- Girardi L., Chiosi C., Bertelli G., Bressan A., 1995, *A&A*, 298, 87
- Gorjian V., 1996, *AJ*, 112, 1886
- Harris W. E., van den Bergh S., 1981, *AJ*, 86, 1627
- Harris W. E., 1991, *ARA&A*, 29, 543
- Harris W. E., 1996, *AJ*, 112, 1487
- Harris W. E., Pudritz R. E., 1994, *ApJ*, 429, 177
- Hippelein H. et al., 1996, *A&A*, 315, L79
- Holtzman J. A., Burrows C. J., Casertano S., Hester J. J., Trauger J. T., Watson A. M., Worthey G., 1995, *PASP*, 107, 1065
- Kennicutt R. A., 1998a, *ARA&A*, 36, 189
- Kennicutt R. A., 1998b, *ApJ*, 498, 541
- Krist J., Hook R., 1997, "The Tiny Tim User's Guide", *STScI*
- Lada E. A., Evans II N. J., Falgarone E., 1997, *ApJ*, 488, 286
- Landolt A. U., 1992, *AJ*, 104, 340
- Larsen S. S., 1999, *A&AS*, 139, 393
- Larsen S. S., 1999, Ph.D. thesis, Copenhagen University Observatory
- Larsen S. S., Richtler T., 2000, *A&A*, 354, 836
- McKee C. F., 1999, in: The origin of stars and planetary systems, Eds. C. J. Lada and N. D. Kylafis, Kluwer Academic Publishers
- Meurer G. R., Heckman T. M., Leitherer C., Kinney A., Robert C., Garnet D. R., 1995, *AJ*, 110, 2665
- O'Connell R. W., Gallagher III J. S., Hunter D. A., Colley W. N., 1995, *ApJL*, 446, 1
- Okamura S., Kanazawa T., Kodaira K., 1976, *PASJ*, 28, 329
- Rand R. J., Kulkarni S. R., 1990, *ApJL*, 349, 43
- Rand R. J., Lord S. D., Higdon J. L., 1999, *ApJ*, 513, 720
- Rice W., Lonsdale C. J., Soifer B. T., Neugebauer G., Koplan E. L., Lloyd L. A., de Jong T., Habing H. J., 1988, *ApJS*, 68, 91
- Schlegel D. J., Finkbeiner D. P., Davis, M., 1998, *ApJ*, 500, 525
- Schmidt-Kaler T., 1967, *AJ*, 72, 526
- Smith J., 1982, *ApJ*, 261, 463
- Stetson P. B., 1987, *PASP*, 99, 191
- Tully R. B., 1974, *ApJS*, 27, 437
- van den Bergh S., 1978, *A&A*, 63, 275
- van den Bergh S., Lafontaine A., 1984, *AJ*, 89, 1822
- van den Bergh S., 1991, *ApJ*, 369, 1
- Vogel S. N., Kulkarni S. R., Scoville N. Z., 1988, *Nature*, 334, 402
- Whitmore B. C., Zhang Q., Leitherer C., Fall S. M., Schweizer F., Miller B. W., 1999, *AJ*, 118, 1551
- Wilson C. D., Scoville N., Madden S. C., Charmandaris V., 2000, *ApJ* (in press), astro-ph/0005208
- Wyder T. K., Hodge P. W., Cole A., 2000, *PASP*, 112, 594
- Xilouris E. M., Byun Y. I., Kylafis N. D., Paleologou E. V., Papamastorakis J., 1999, *A&A*, 344, 868
- Zepf S. E., Ashman K. M., English J., Freeman K. C., Sharples R. M., 1999, *AJ*, 118, 752



**Table 3.** Data for clusters in M51.  $M_V$ ,  $U-B$  and  $B-V$  have been corrected for a foreground extinction of  $A_B = 0.150$  mag. Clusters marked with an asterisk (\*) were included on the HST F439W and F555W pointings.

| ID   | RA(2000.0)  | DEC(2000.0) | $M_V$  | $U-B$ | $B-V$ |
|------|-------------|-------------|--------|-------|-------|
| 27   | 13:29:35.09 | 47:12:12.5  | -9.32  | -0.36 | 0.38  |
| 31   | 13:29:35.70 | 47:10:44.4  | -9.51  | -0.38 | 0.30  |
| 37   | 13:29:36.54 | 47:09:13.0  | -10.51 | -0.84 | 0.30  |
| 41   | 13:29:36.80 | 47:11:19.3  | -10.24 | -0.48 | 0.29  |
| 46   | 13:29:37.14 | 47:10:04.2  | -10.09 | -0.56 | 0.39  |
| 61   | 13:29:38.31 | 47:11:05.1  | -10.42 | -0.65 | 0.19  |
| 84   | 13:29:39.78 | 47:10:32.9  | -10.62 | -0.69 | 0.17  |
| 92   | 13:29:40.04 | 47:09:24.0  | -9.58  | -0.35 | 0.28  |
| 94   | 13:29:40.16 | 47:10:43.8  | -10.37 | -0.65 | 0.14  |
| 101  | 13:29:40.57 | 47:11:51.2  | -10.82 | -0.34 | 0.28  |
| 111  | 13:29:41.27 | 47:13:25.8  | -9.46  | -0.17 | 0.37  |
| 122  | 13:29:41.85 | 47:11:42.6  | -10.43 | -0.42 | 0.20  |
| 130  | 13:29:42.40 | 47:13:19.0  | -9.58  | -0.46 | 0.18  |
| 162  | 13:29:43.64 | 47:10:48.5  | -9.66  | -0.74 | 0.17  |
| 172  | 13:29:43.90 | 47:09:55.6  | -10.92 | -0.92 | 0.32  |
| 176  | 13:29:43.99 | 47:09:32.8  | -9.68  | -0.97 | 0.37  |
| 180  | 13:29:44.13 | 47:10:23.7  | -12.46 | -1.11 | 0.07  |
| 203  | 13:29:44.94 | 47:09:59.4  | -12.82 | -1.08 | 0.08  |
| 263  | 13:29:46.52 | 47:12:33.5  | -11.45 | -0.97 | 0.06  |
| 320  | 13:29:48.09 | 47:13:32.9  | -8.80  | -0.37 | -0.02 |
| 330  | 13:29:48.47 | 47:13:19.6  | -9.72  | -0.67 | 0.32  |
| 335  | 13:29:48.73 | 47:13:34.7  | -9.61  | -0.68 | 0.05  |
| 368  | 13:29:49.95 | 47:08:34.3  | -9.00  | -0.34 | 0.32  |
| 395  | 13:29:50.66 | 47:10:07.1  | -11.12 | -0.88 | 0.11  |
| *403 | 13:29:50.83 | 47:10:41.4  | -10.13 | -0.84 | 0.34  |
| 409  | 13:29:51.15 | 47:09:18.0  | -9.87  | -0.92 | 0.11  |
| 416  | 13:29:51.47 | 47:10:10.1  | -9.57  | -0.79 | 0.11  |
| 420  | 13:29:51.67 | 47:09:09.2  | -10.46 | -0.89 | 0.19  |
| 422  | 13:29:51.69 | 47:08:52.9  | -9.69  | -0.95 | 0.15  |
| 459  | 13:29:52.77 | 47:09:12.7  | -9.84  | -0.92 | 0.34  |
| *477 | 13:29:53.22 | 47:12:39.7  | -11.30 | -0.77 | 0.21  |
| *479 | 13:29:53.30 | 47:10:42.9  | -11.60 | -0.90 | 0.10  |
| 495  | 13:29:53.83 | 47:12:57.7  | -9.94  | -0.21 | 0.31  |
| *534 | 13:29:54.88 | 47:12:50.6  | -10.23 | -0.79 | 0.18  |
| 559  | 13:29:55.55 | 47:14:02.5  | -11.58 | -1.01 | 0.01  |
| *589 | 13:29:56.30 | 47:12:43.2  | -10.31 | -0.74 | 0.07  |
| *597 | 13:29:56.55 | 47:10:47.6  | -9.81  | -0.77 | 0.18  |
| *627 | 13:29:57.05 | 47:11:31.7  | -9.58  | -0.99 | 0.24  |
| 649  | 13:29:57.64 | 47:09:32.5  | -9.21  | -0.12 | 0.26  |
| 684  | 13:29:58.48 | 47:13:49.4  | -10.63 | -1.07 | -0.09 |
| *693 | 13:29:58.65 | 47:12:58.3  | -10.29 | -0.59 | 0.15  |
| *713 | 13:29:58.96 | 47:11:04.7  | -11.38 | -0.98 | 0.07  |
| 747  | 13:29:59.70 | 47:13:40.6  | -11.29 | -0.94 | 0.04  |
| 750  | 13:29:59.70 | 47:13:59.2  | -12.54 | -0.96 | 0.04  |
| 759  | 13:29:59.90 | 47:09:36.3  | -9.36  | -0.22 | 0.40  |
| 803  | 13:30:00.60 | 47:13:27.0  | -10.93 | -0.79 | 0.12  |
| 832  | 13:30:00.97 | 47:09:29.5  | -10.86 | -1.37 | 0.05  |
| 839  | 13:30:01.12 | 47:13:45.3  | -11.09 | -0.81 | 0.02  |
| 842  | 13:30:01.27 | 47:16:53.9  | -10.62 | -0.72 | 0.20  |
| 848  | 13:30:01.32 | 47:12:51.5  | -11.52 | -0.97 | 0.03  |
| 852  | 13:30:01.35 | 47:09:12.6  | -8.53  | -0.01 | 0.23  |
| 872  | 13:30:01.84 | 47:15:34.4  | -10.19 | -0.28 | 0.36  |
| 883  | 13:30:02.11 | 47:13:26.1  | -10.78 | -0.67 | 0.08  |
| 890  | 13:30:02.25 | 47:12:33.1  | -10.31 | -0.51 | 0.12  |
| 899  | 13:30:02.43 | 47:09:49.6  | -12.18 | -1.12 | 0.20  |
| 911  | 13:30:02.78 | 47:09:57.3  | -10.99 | -1.18 | 0.16  |
| *912 | 13:30:02.82 | 47:11:30.1  | -9.93  | -0.58 | 0.32  |
| 924  | 13:30:03.18 | 47:12:45.5  | -11.01 | -1.00 | -0.01 |
| 936  | 13:30:03.81 | 47:12:00.9  | -9.60  | -0.96 | 0.04  |
| 947  | 13:30:03.97 | 47:10:15.3  | -11.18 | -0.87 | 0.13  |

Table 3 (continued)

| ID   | RA(2000.0)  | DEC(2000.0) | $M_V$  | $U-B$ | $B-V$ |
|------|-------------|-------------|--------|-------|-------|
| 984  | 13:30:05.03 | 47:12:33.1  | -11.12 | -0.88 | 0.08  |
| 987  | 13:30:05.04 | 47:10:18.6  | -9.52  | -1.03 | 0.07  |
| 993  | 13:30:05.19 | 47:10:50.5  | -8.85  | -0.22 | 0.27  |
| 1013 | 13:30:05.70 | 47:09:49.9  | -9.90  | -0.32 | 0.27  |
| 1019 | 13:30:05.92 | 47:11:40.5  | -9.82  | -0.62 | 0.35  |
| 1031 | 13:30:06.55 | 47:11:01.1  | -9.51  | -0.75 | 0.21  |
| 1033 | 13:30:06.67 | 47:14:20.7  | -11.57 | -0.86 | 0.08  |
| 1049 | 13:30:07.40 | 47:11:26.5  | -10.12 | -1.01 | 0.03  |
| 1066 | 13:30:08.47 | 47:13:59.7  | -9.34  | -0.22 | 0.36  |